

Future Health Impacts from Climate Change in Rhode Island: Evidence from Climate Models

**Prepared for
Rhode Island Department of Health**

Prepared by



**One Park Drive, Suite 200 • PO Box 14409
Research Triangle Park, NC 27709**

October 25, 2013

(This page intentionally left blank)

Contents

1	Executive Summary.....	1
2	Future Climate Projections	3
2.1	Climate Scenarios.....	3
2.1.1	Downscaling and the Delta Method.....	4
2.1.2	Selected Global Circulation Models (GCMs).....	4
2.1.3	Projected Temperature Changes	5
2.2	Heat Islands and Green Space	10
2.3	Land Use Projections	11
3	Heat and Humidity: Projected Changes.....	13
4	Heat Variability	17
5	Pollen and Allergens.....	19
6	Disease Vectors and Climate.....	21
6.1	Ticks and Lyme Disease.....	21
6.2	Mosquitoes and West Nile Virus.....	23
7	Conclusions.....	27
8	References	29
	Appendix A. Heat Index Calculation.....	32
	Appendix B. Relative Humidity Calculation.....	33

Tables

Table 1. Selected GCM Models, Emission Pathways, and Projection Run Numbers	5
Table 2. Interpretation of the Heat Index (NWS 2013)	13
Table 3. Average Number of Heat Advisories per Year by Model Scenario for Current, 2022, 2052, and 2084 Time Horizons	16
Table 4. Hazard Ratio for a 1 °C Increase in Yearly Summer Temperature <i>SD</i> by Climate Region.....	17
Table 5. Length of Aeroallergen Production Season, Median of Climate Model Projections	20
Table 6. Projected Minimum Infection Ratio (MIR, %) for West Nile Virus in <i>Culex</i> Mosquitoes under Baseline and Future Climate Scenarios W1–W8 (July–September Average)	25

Figures

Figure 1. The 24 climate scenarios.	3
Figure 2. Modeled air temperature for 2022 conditions compared to 1978–2007 baseline.	6
Figure 3. Modeled air temperature for 2052 conditions compared to 1978–2007 baseline.	6
Figure 4. Modeled air temperature for 2084 conditions compared to 1978–2007 baseline.	7
Figure 5. Monthly variation of modeled temperature for 2022 conditions compared to 1978–2007 baseline.	7
Figure 6. Monthly variation of modeled temperature for 2052 conditions compared to 1978–2007 baseline.	8
Figure 7. Monthly variation of modeled temperature for 2084 conditions compared to 1978–2007 baseline.	8
Figure 8. ICLUS-projected change in impervious cover by county.	11
Figure 9. NWS Heat Index chart including hazard zones (NWS 2013).	14
Figure 10. Heat advisories per year, averaged across all scenarios.	16
Figure 11. Length of growing season predicted by SWAT for the 1978–2007 baseline and eight climate change scenarios centered at 2084.	20
Figure 12. Predicted density of deer tick population in Rhode Island relative to current climate conditions.	23
Figure 13. Example minimum infection ratio (MIR) for West Nile Virus in <i>Culex</i> mosquitos, baseline simulation for 2008.	24
Figure 14. Projected time course of minimum infection ratio (MIR) for West Nile Virus in <i>Culex</i> Mosquitoes under Baseline and Future Climate Scenarios (July–September Average)	25

(This page intentionally left blank)

1 Executive Summary

The Rhode Island Department of Health is charged with identifying potential risks to human health that may result from climate change. This report provides technical information in support of that goal.

Tetra Tech previously developed and assembled information on potential changes in Rhode Island's climate for *SafeWater RI: Phase 2 Report, Assessment of Impacts* (Tetra Tech 2012). *SafeWater RI* studied the impacts of climate change on drinking water utilities in the state and provided specific information for water utility managers to evaluate and plan for the future. As part of that project, data were assembled for 24 future climate scenarios using a variety of climate simulation models, greenhouse gas (GHG) emissions scenarios, and three future time horizons through the end of the 21st century. The same climate information can also inform us about a number of impacts on human health.

An altered climate may impact human health in a variety of ways. This report focuses on future health impacts due to climate change, including impacts that arise from increased temperatures, such as heat stroke; influences of climate change on disease vectors, such as mosquitoes and ticks; and aeroallergen pollen production. An accompanying report will present physical hazards associated with extreme weather and sea level rise.

The heat and humidity assessment suggests that the average number of days with "Danger" heat advisories, when heat cramps and heat exhaustion are likely, may increase from less than 1 to more than 4 days per year by 2084. The projected temperature increases will also affect daily life, limiting the time people can spend outdoors during the summer and increasing energy use because of a greater need for air conditioning. Additionally, climate projections suggest earlier spring blooms and later fall frosts, resulting in a lengthening of the allergy season in Rhode Island. As temperatures rise and summers become longer, ticks and mosquitos will remain active for longer periods of time and likely increase in numbers, leading to increased risk of Lyme disease, West Nile Virus, and other vector-borne diseases. Note that nymphal deer tick abundance in Rhode Island is determined by relative humidity levels in June. Higher humidity means greater tick survival, more tick encounters and more disease. If the future climate in Rhode Island is a more humid one, this could create the ideal habitat for ticks.

Available climate projections suggest that climate-related risks to the health of Rhode Island citizens will increase over the coming years. It is important to note that the results of this report are only preliminary estimates of future trends, and the possible range of futures, to which adaptation may be needed. Rhode Island must continue to monitor climate changes to further understand immediate and future impacts. The human health impacts discussed in this report will require that Rhode Island develop adaptation strategies geared toward protecting its citizens' health into the future.

(This page left intentionally blank.)

2 Future Climate Projections

To assess the impacts of future temperature and extreme weather on human health, Tetra Tech used Global Climate Models (also referred to as General Circulation Models, or GCMs), which are computer simulations that use mathematical equations to predict future climate. As Section 2.1 explains, these GCMs were combined with greenhouse gas (GHG) emissions scenarios to develop a range of possible future climates. This process provides an array of potential air temperatures and precipitation trends that are used to predict the frequency of extreme heat and weather events.

This analysis builds on data that Tetra Tech initially developed and assembled for *SafeWater RI: Phase 2 Report, Assessment of Impacts* (Tetra Tech 2012). *SafeWater RI* studied the impacts of climate change on drinking water utilities in the state and provided specific information for water utility managers to evaluate and plan for the future. The analysis for *SafeWater RI* evaluated a suite of future climate scenarios to understand the potential range of changes in air temperature and precipitation for the state. The methodology included detailed analyses of weather station records in Providence and Kingston, along with projections of land use change across the state. The *SafeWater RI* data sets have been further applied here to evaluate the impacts that climate change could have on human health.

2.1 CLIMATE SCENARIOS

The goal of the climate change assessment is not to determine the single, *most likely* future trajectory, but instead to better understand the range of conditions to which we might need to adapt. This method

addresses the inherent uncertainties of climate prediction by using an approach that evaluates a number of scientifically plausible future states and includes an assessment of the sensitivity of the system. For this project, 24 climate scenarios were identified for evaluation (Figure 1). The 24 scenarios are based on four GCMs, which were applied to three future time periods (2022, 2052, and 2084) and under two different GHG emissions scenarios (A2 and B1).

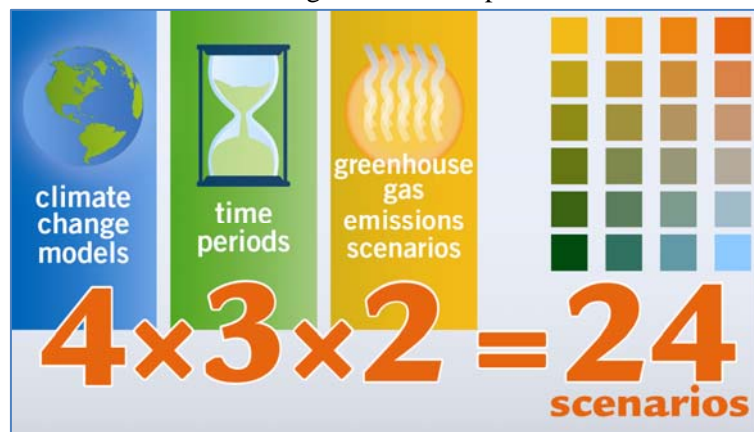


Figure 1. The 24 climate scenarios.

The projected climate scenarios are derived using GCMs, run with projections of future GHG concentrations that drive atmospheric warming, as summarized in the *Special Report on Emissions Scenarios* (Nakicenovic et al. 2000). The GCMs estimate future temperature and precipitation conditions using a three-dimensional grid over the globe. Those used in this analysis are on a grid scale of around 100 kilometers (km) by 100 km. A technique called *downscaling* is used to convert these global estimates to a smaller spatial scale that represents regional dynamics and regionally specific climate forecasts (i.e., specific to Rhode Island). It should be made clear that there are many uncertainties related to current understanding of the physical climate system and future GHG emissions. Although we cannot predict the exact conditions that will be faced in future decades, it is clear that temperatures will, on average, be warmer. The 2007 Fourth Assessment Report of the Intergovernmental Panel on Climate Change (IPCC) states that warming of the climate system is now “unequivocal” (IPCC 2007). Climate modeling experiments suggest these trends will continue throughout the 21st century, with continued warming accompanied by a general intensification of the global hydrologic cycle (IPCC 2007; Karl et al. 2009).

2.1.1 Downscaling and the Delta Method

The temperature and precipitation projections from the GCMs are useful for broad assessments of global climate change, but they do not provide precise estimates of climate changes at the local level. Additionally, GCMs tend to generate too many low-intensity events and under-simulate the intensity of large events (Sun et al. 2006; Dai 2006), downplaying the strength of many future climate impacts. These problems can be addressed by downscaling the GCM output to a smaller spatial scale and by implementing the GCM predictions using a change factor or delta method (Anandhi et al. 2011) in which historical time series are modified to reflect the relative changes in precipitation and temperature predicted by the GCM. This ensures that the resulting meteorological series are physically realistic at the local scale.

The World Climate Research Programme's (WCRP's) Coupled Model Intercomparison Project Phase 3 (CMIP3) Bias-Corrected and Spatially Downscaled¹ (BCSD) data was used for downscaling. These products use statistical bias correction to interpret GCMs over a large spatial domain on the basis of results from current observation stations. The BCSD products provide time series for precipitation and temperature as computed by a given GCM for future time horizons, as well as historical analysis. Change factors are calculated by comparing a future time slice of 30 years to the 1978–2007 output of the same model on a monthly basis. Multiplicative factors are developed for precipitation, and additive factors are developed for air temperature. These are then used to construct a future analog of the observed climate series for 1978–2007.

2.1.2 Selected Global Circulation Models (GCMs)

Four GCMs under two emissions scenarios were selected for this project's analysis. The A2 and B1 emission storylines were selected because they represent a range of higher and lower GHG emissions.² Emissions scenarios describe future releases into the atmosphere of greenhouse gases and other pollutants, and they include changes in land use and land cover. Each scenario is based on different assumptions about patterns of economic and population growth, technology development, and other factors. Because levels of future emissions are highly uncertain, these emissions scenarios provide alternative snapshots of how the future might unfold. Sixteen CMIP3 models are available under each emissions scenario, with each model having one or more simulations consisting of unique initial conditions or runs.³ The GCMs selected for this project were CGCM3, GFDL, CCSM3, and HadCM3. They were selected because of their international recognition and use and because they provided higher data availability than other GCMs.

Table 1 shows the selected emission pathways, GCMs, and run numbers (index of the model run in the climate data archive).

¹ The BCSD climate projection archive is available at <http://gdo-dcp.ucllnl.org> and includes data sets representing three scenarios for future GHG emissions, as defined in Nakicenovic et al. (2000).

² The A2 emissions scenario assumes a very heterogeneous world with continuously increasing global population and regionally oriented economic growth that is more fragmented and slower than in other storylines. The B1 scenario family is near the lower limit of projected changes in GHG emissions. The B1 scenario assumes global population growth peaks by mid-century and then declines, a rapid economic shift toward service and information economies, and the introduction of clean and resource-efficient technologies. For more information on emissions scenarios, see the IPCC website at <http://sedac.ipcc-data.org/ddc/sres/index.html>.

³ For more information on the World Climate Research Programme Coupled Model Intercomparison Project Phase 3, see http://www.ipcc.ch/publications_and_data/ar4/wg1/en/ch10s10-1.html.

Table 1. Selected GCM Models, Emission Pathways, and Projection Run Numbers

Modeling group, country	WCRP CMIP3 I.D.	BCSD CMIP3 climate and hydrologic projections	
		SRES A2 run #	SRES B1 run #
Canadian Centre for Climate Modeling & Analysis	CGCM3.1 (T47)	4	4
U.S. Department of Commerce/NOAA/Geophysical Fluid Dynamics Laboratory, USA	GFDL-CM2.0	1	1
National Center for Atmospheric Research, USA	CCSM3	4	4
Hadley Centre for Climate Prediction and Research/ Met Office, United Kingdom	UKMO-HadCM3	1	1

Source: Nakicenovic et al. 2000.

Notes: NOAA = National Oceanic and Atmospheric Administration; WCRP = World Climate Research Program; CMIP3 = Coupled Model Intercomparison Project phase 3; BCSD = Bias-Corrected and Spatially Downscaled; SRES = Special Report on Emissions Scenarios.

The BCSD-CMIP3 climate projections are available at a resolution of 1/8° latitude-longitude (~12 km by 12 km). The available time series output covers a 150-year period from 1950 through 2099.

Current baseline conditions are represented by a 30-year period from 1978 through 2007. The observed time series were then modified using the delta method, described below, to create comparable 30-year time series for future time horizons. A 30-year basis was selected to provide a good representation of the natural variability and decadal oscillations in the climate and hydrology of the watershed. The three future time horizons centered on 2022, 2052, and 2084 were compared to the base period to modify the weather time series as follows:

- Time Horizon 1 centered at 2022: Compare 2008–2037 to 1978–2007
- Time Horizon 2 centered at 2052: Compare 2038–2067 to 1978–2007
- Time Horizon 3 centered at 2084: Compare 2070–2099 to 1978–2007

Multiyear monthly averages for air temperature and precipitation were first calculated for each time slice, including the base or current period. For each of the 24 climate scenarios, monthly deltas and percent change statistics were calculated relative to the base period. The deltas were calculated as the future minus the current, and the percent change was calculated as the delta divided by the current.

2.1.3 Projected Temperature Changes

The downscaled climate projections of surface air temperature are presented in the graphs on the following pages (Figures 2 through 7). These graphs are presented as box-and-whisker plots (Figure 2, Figure 3, and Figure 4) and seasonal plots (Figure 5, Figure 6, and Figure 7). The box-and-whisker plots show the 25th percentile, median, and 75th percentile (the box), along with the range from the minimum to the maximum (the whiskers). The seasonal plots show the average for each month over the 30-year simulation. For each time horizon, the eight model-derived series are shown as lines and the existing baseline condition is shown in the background as an area. As time progresses, the seasonal trend graphs show that the range of possible future air temperatures increases (the difference between the climate model output and current conditions is greater in 2052 and 2084 than in 2022).

Temperature predictions for all scenarios increase consistently with each time horizon. Annual average temperature increase for the 2084 scenarios was around 5.7 °F (3.2 °C), whereas for the 2022 scenarios, it was around 1.6 °F (0.9 °C).

Air Temperature (degF) -Time Horizon 2022

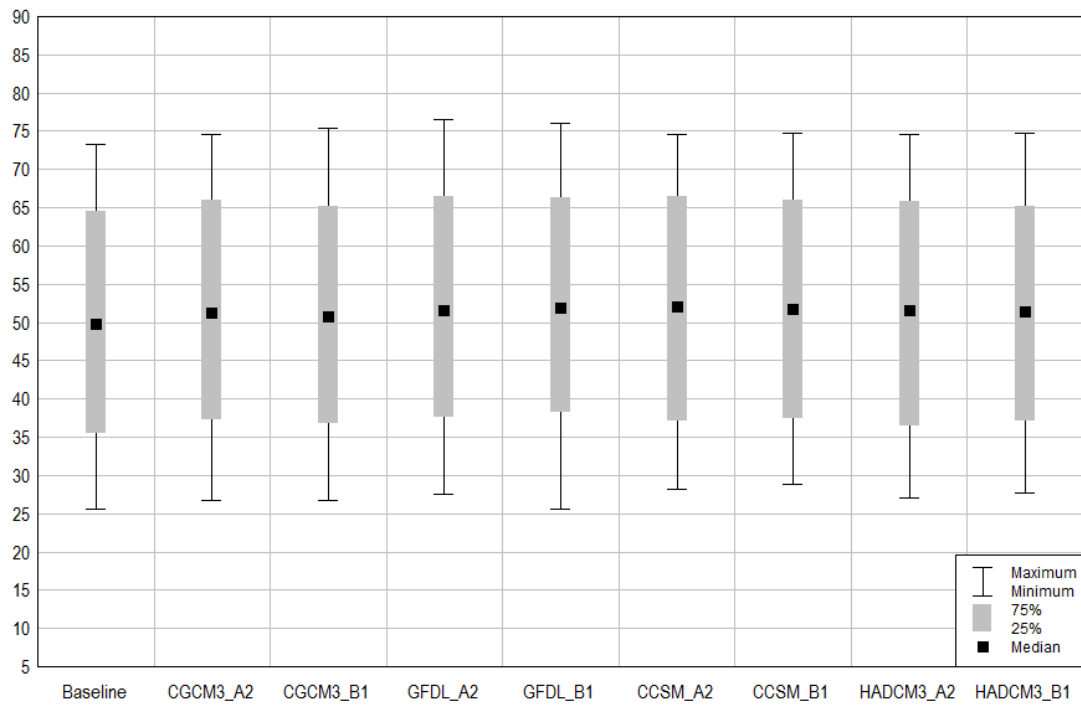


Figure 2. Modeled air temperature for 2022 conditions compared to 1978–2007 baseline.

Air Temperature (degF) -Time Horizon 2052

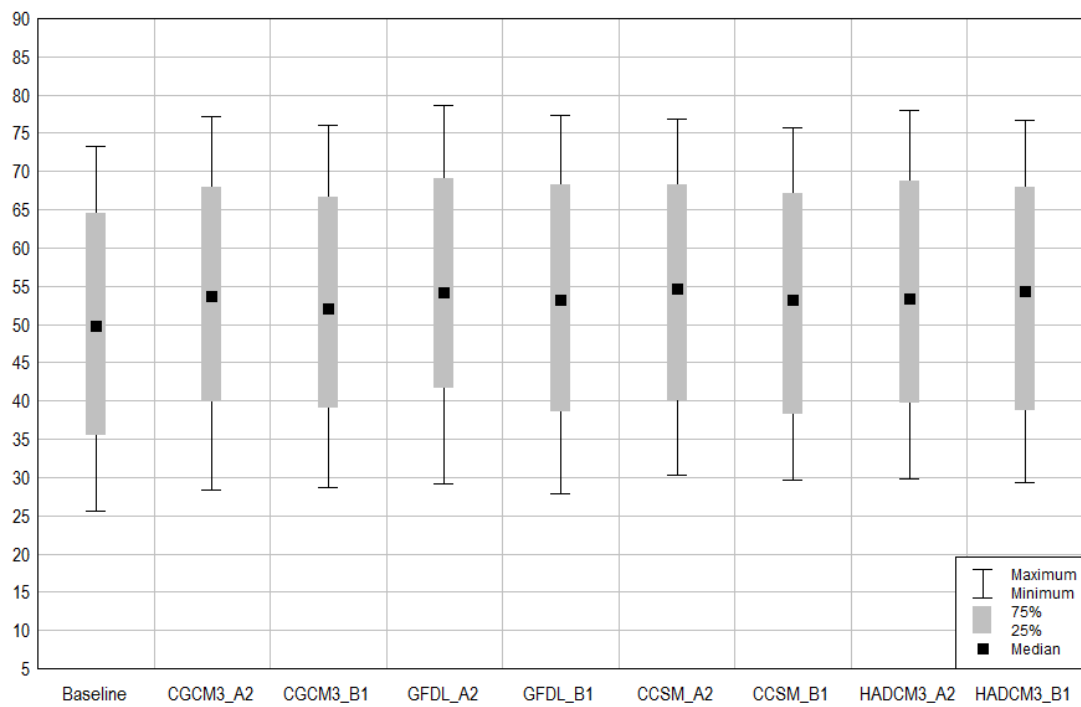


Figure 3. Modeled air temperature for 2052 conditions compared to 1978–2007 baseline.

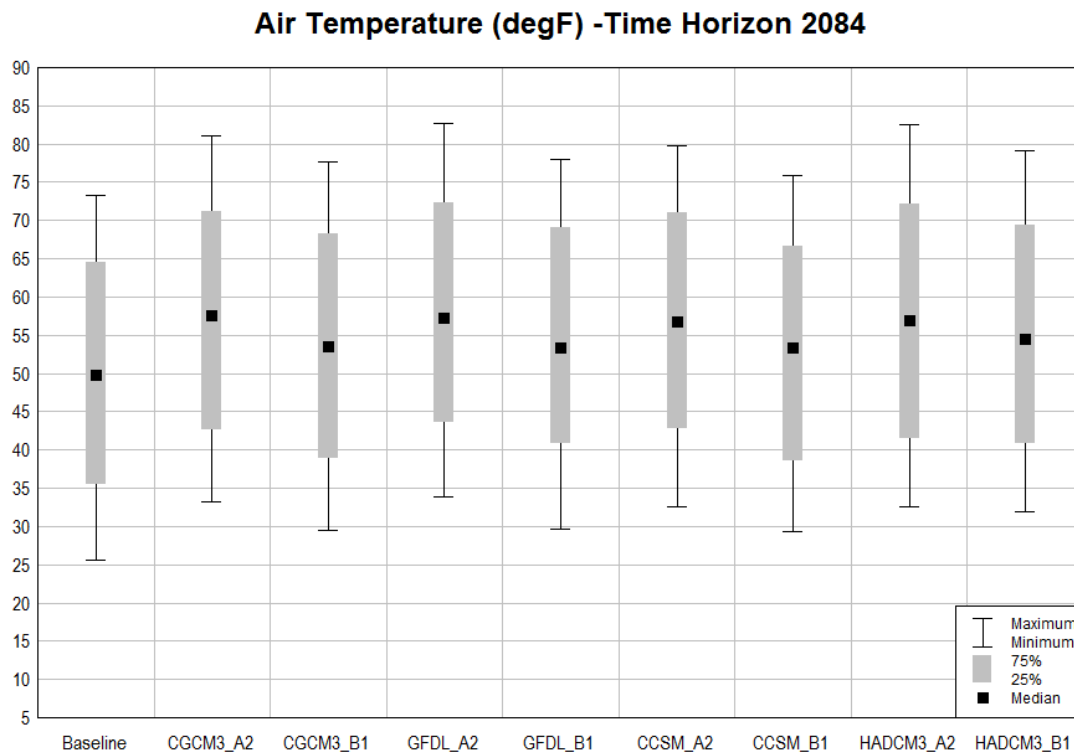


Figure 4. Modeled air temperature for 2084 conditions compared to 1978–2007 baseline.



Figure 5. Monthly variation of modeled temperature for 2022 conditions compared to 1978–2007 baseline.

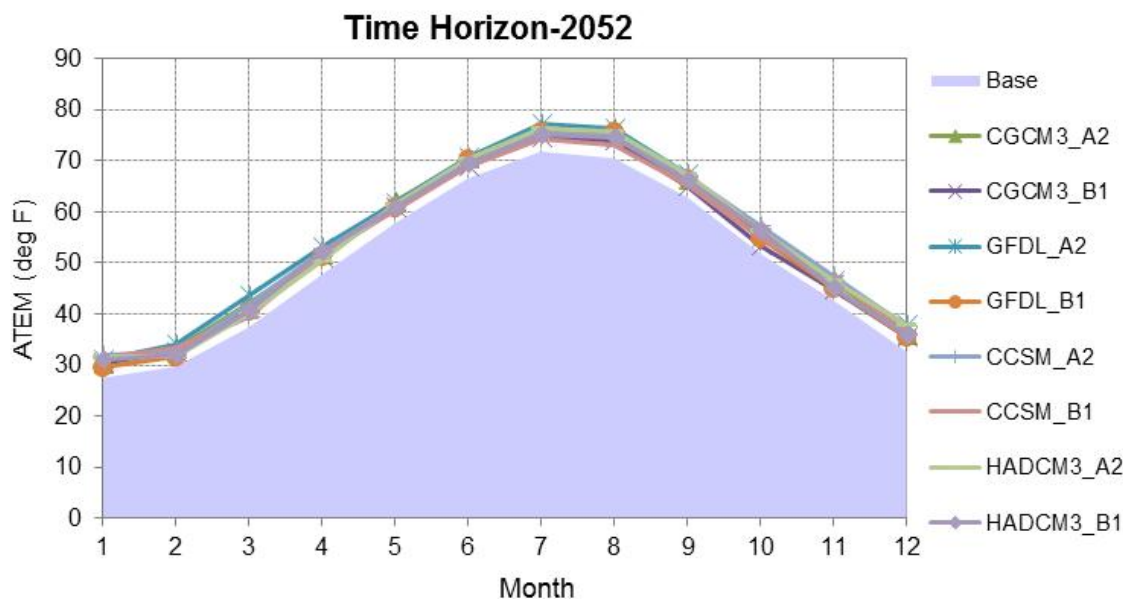


Figure 6. Monthly variation of modeled temperature for 2052 conditions compared to 1978–2007 baseline.

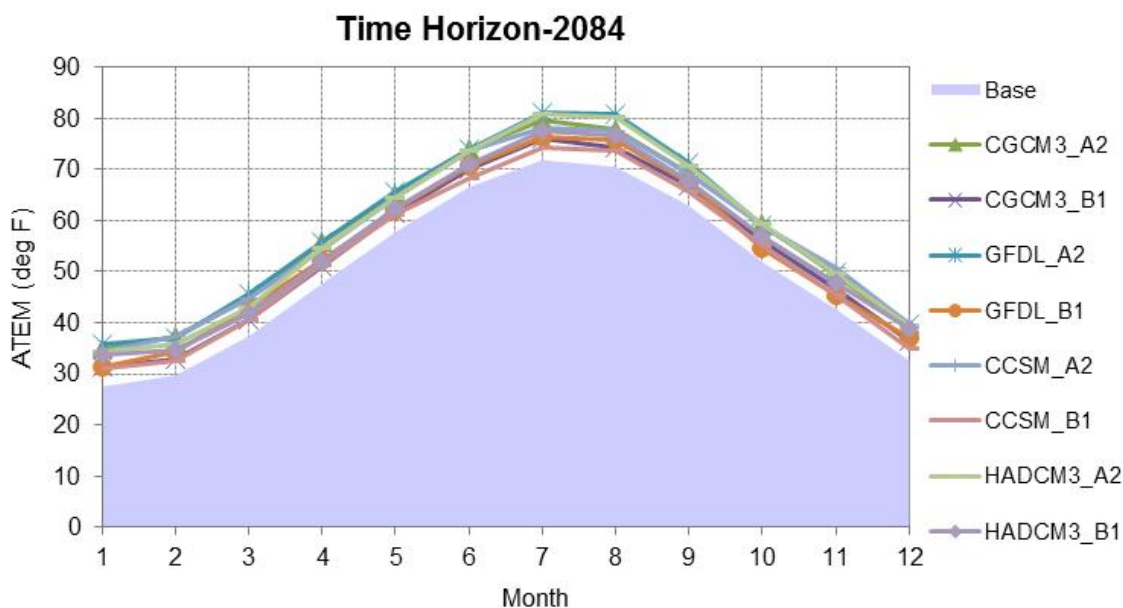


Figure 7. Monthly variation of modeled temperature for 2084 conditions compared to 1978–2007 baseline.

It should be noted that although the GCMs are in agreement in predicting increases in temperature throughout the year, they are often in disagreement as to whether average precipitation will increase or decrease for a given month.

In addition to warmer temperatures in the summer, all climate model projections suggest warmer winter (December – February) air temperatures as well (Table 2, Table 3). The number of days below freezing in each climate scenario reveals warming of winter months to varying degrees of intensity.

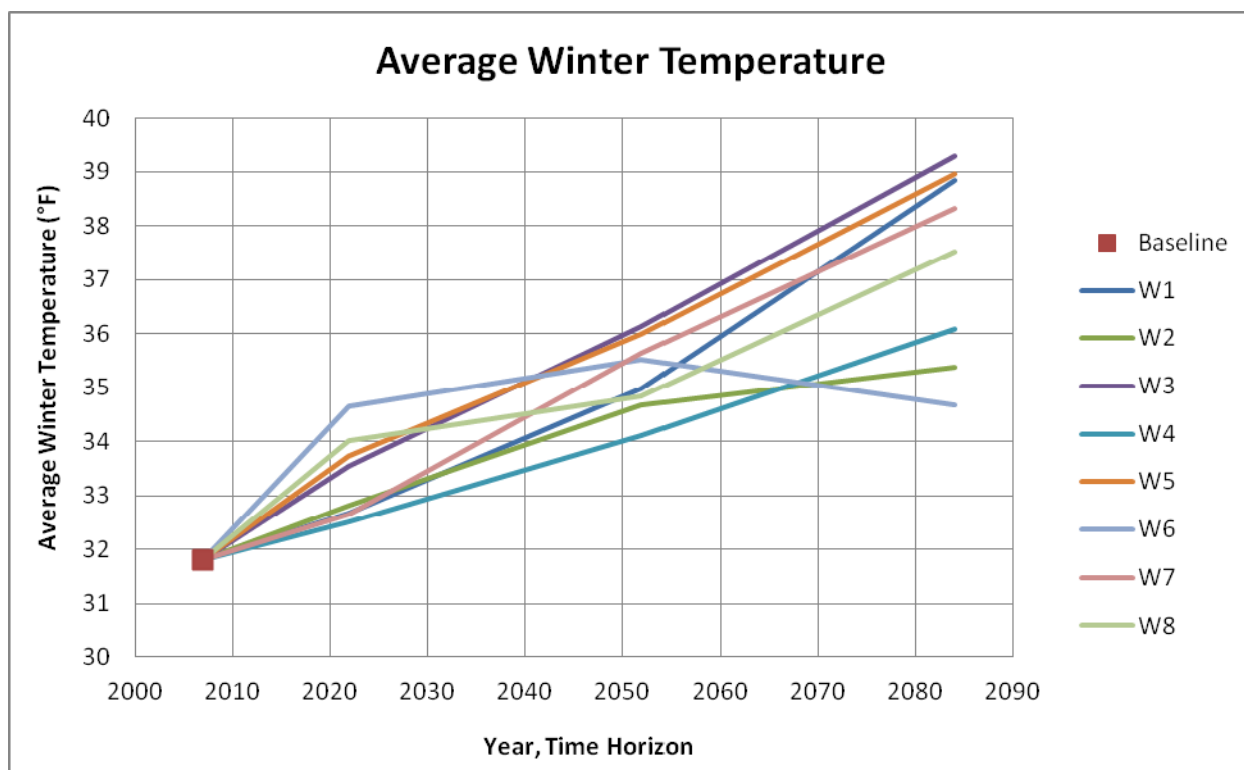
Table 2. Average number of days per year that are below freezing for each climate scenario and time horizon.

Time Horizon	Baseline	W1	W2	W3	W4	W5	W6	W7	W8
2022	52	47	47	44	46	43	40	49	43
2052	52	37	38	32	41	33	36	36	38
2084	52	22	35	21	32	22	38	25	28

Table 3. Percentage of days per year that are below freezing for each climate scenario and time horizon.

Time Horizon	Baseline	W1	W2	W3	W4	W5	W6	W7	W8
2022	14%	13%	13%	12%	13%	12%	11%	13%	12%
2052	14%	10%	10%	9%	11%	9%	10%	10%	10%
2084	14%	6%	10%	6%	9%	6%	10%	7%	8%

The average winter temperature for each scenario as compared to the current average baseline winter temperature shows a consistent pattern of winter warming (Figure 8. Average winter (December – February) air temperature by climate scenario and time horizon. Figure 8). The one exception is in scenario 8, where the winter average air temperature is expected to decline from the 2050s to the 2080s, although remaining well elevated over current conditions.

**Figure 8. Average winter (December – February) air temperature by climate scenario and time horizon.**

2.2 HEAT ISLANDS AND GREEN SPACE

Highly impervious built environments can further amplify heat (the “heat island” effect), while urban green space (with shade and evaporative cooling) can mitigate heat. The annual mean air temperature of a city with 1 million people or more can be anywhere from 1.8 to 5.4°F warmer than its surroundings. In the evening, the difference can be as high as 22 °F (USEPA 2008a). The differences are largely due to the sun’s rays heating up impervious surfaces, such as roads, parking lots, and roofs. For instance, in a detailed study on thermal regimes in urban parks in Vancouver, British Columbia, rooftop temperatures were measured at 113–131 °F (45–55 °C) and road and parking lot pavement temperatures at 97–100 °F (36–38 °C), while tree canopies and shaded ground were near the air temperature of 73 °F (23 °C) (Spronken-Smith and Oke 1998).

The increased temperatures in urban heat islands can amplify the temperature increases projected by climate models, which do not resolve the spatial scale of city blocks. This is especially of concern because heat island effects are often correlated to areas of high population density and lower socioeconomic status that may increase temperature-associated health risks. In addition, Zanobetti et al. (2012) found that increases in green surface within a ZIP Code correlated with decreases in the hazard ratio (HR) for adverse health outcomes to increased summer temperature *SD*. Thus, land use, and land use change, will interact with climate to affect health outcomes.

The Integrated Climate and Land Use Scenarios (ICLUS) land use projections, which estimate residential density and imperviousness consistent with the emissions scenario storylines used in climate modeling, provide an indication of the potential for changes in urban density (see Section 2.3). It should be noted that this does not reveal direct information on future heat island effects or green space because it does not account for policy and urban design choices. It also does not account for potential changes in commercial and industrial density. Nonetheless, the gross projections of potential changes in residential impervious area are informative as to the degree to which planning and adaptation may be needed to address heat island effects.

ICLUS projections are available for each decade in the 21st century. Therefore, this report examined results for 2010, 2050, and 2090 (Figure 9). Little change in impervious cover is forecast for Bristol, Kent, and Newport counties. However, impervious cover is projected to increase from 6.7 to 9.8 percent in suburban Washington County, and from 12.8 to 20.7 percent in largely urban Providence County. Thus, significant effort may be needed to mitigate potential heat island effects in the Providence metropolitan area.

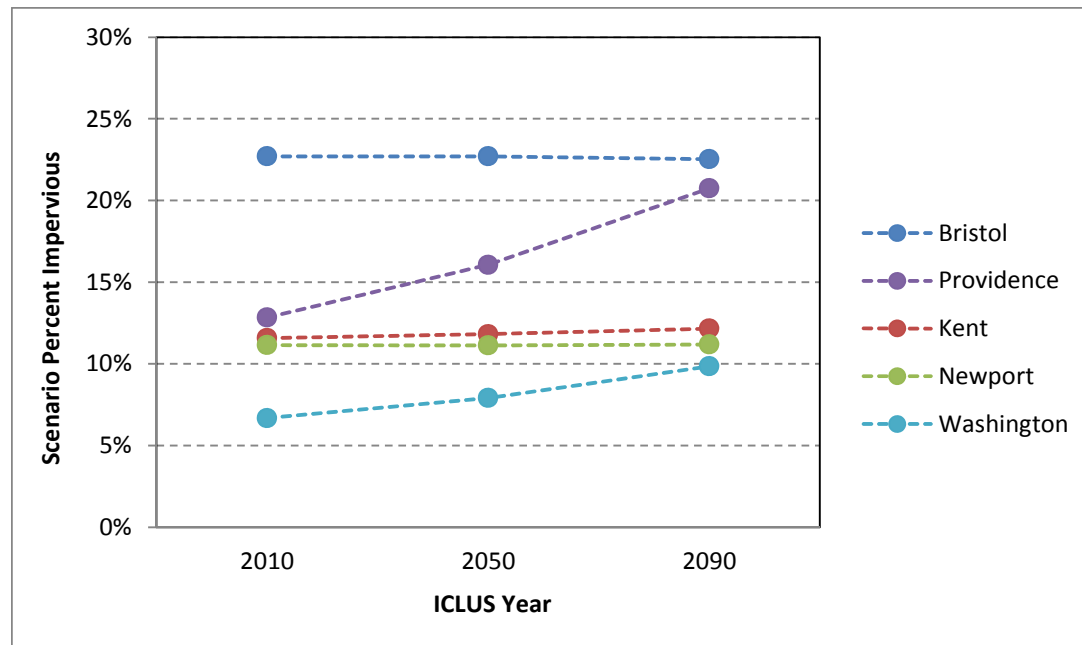


Figure 9. ICLUS-projected change in impervious cover by county.

2.3 LAND USE PROJECTIONS

Altering a region's natural vegetation has the potential to modify the prevailing surface temperatures, humidity, and energy fluxes. Furthermore, impact assessments frequently show that interactions between climate and land use changes can create serious challenges for aquatic ecosystems, water quality, and air quality (USEPA 2013b). It is therefore important to evaluate climate and land use change in concert when assessing future environmental changes, particularly future temperature variations.

On hot days, the sun can heat exposed urban surfaces, such as roofs and pavement, to temperatures 50–90 °F (27–50 °C) hotter than the air, while shaded or moist surfaces remain close to air temperatures. Understanding the amount of urban and residential development projected for Rhode Island is critical to estimating how local temperatures will change in the coming years.

Projected changes in urban and residential development used in this analysis were acquired from EPA's ICLUS project (USEPA 2009). ICLUS has produced seamless, national-scale change scenarios for developed land that are compatible with the assumptions about population growth, migration, and economic development that underlie the IPCC greenhouse gas emissions storylines. ICLUS projections were developed using a demographic model that distributes the population as housing across the landscape for the four main emissions storylines and a base case. The resulting population is allocated to 1-hectare pixels, by county, using the spatial allocation model SERGoM (Spatially Explicit Regional Growth Model). The model is run for the contiguous United States, and output is available for each scenario by decade to 2100. The final spatial data set provides decadal projections of housing density and impervious surface cover as a function of housing density projections for the period 2000 through 2100 (USEPA 2009).

Data from the ICLUS project are composed of grid-based housing density estimates with 100-meter cells, whose values are set equal to *units/ha x 1,000*. Existing housing densities were estimated using a variety of sources and models, and future housing densities were developed under various scenarios for each decade through 2100. Residential development was not simulated for protected lands (including land placed in conservation easements) and land that is in commercial/industrial under current conditions.

The ICLUS projections are based on changes in residential land areas and do not account for potential growth in commercial/industrial land use. It is also important to note that the ICLUS projections do not explicitly account for changes in rural or agricultural land uses. These categories change in analysis based on ICLUS only when they convert to developed land. The ICLUS projections are an important piece in understanding how local temperature will change into the future.

As communities develop and expand, changes occur in their landscapes. Buildings, roads, homes, and other infrastructure replace open land and forests. Increases in the amount of impervious surfaces, coupled with rising air temperatures, will likely impact water quality in Rhode Island. When rainfall is prevented from slowly filtering into the ground, this stormwater runs swiftly across the landscape, picking up pollutants and debris as it travels to local waterways. Longer periods of warmer temperatures could also result in the proliferation of nuisance algal growth in nutrient-rich streams, lakes, and ponds, when combined with increased stormwater pollution and decreased flushing. Additionally, higher air temperatures translate into warmer runoff and thermal conditions that adversely affect some aquatic life and can increase the occurrence of some water-borne diseases.

3 Heat and Humidity: Projected Changes

Heat exposure can cause a range of negative health effects, from mild heat rashes to deadly heat stroke, depending on the amount of direct sun exposure, humidity, and temperature. Heat can also exacerbate numerous chronic diseases, such as cardiovascular and respiratory disease.

One of the most obvious potential health impacts of climate change is direct stress from increased air temperature. However, direct health impacts also result from the combined effects of heat and humidity. This is because the human body attempts to release excess heat through perspiration (sweating), but that works only if the water that is expressed through the skin evaporates. When the air has a high vapor concentration, it is harder for the air to absorb the sweat from our skin. Therefore, high humidity does not allow the maximum amount of evaporation from the body to occur. This results in a lower rate of heat removal from the body and a greater potential for heat-related illness.

To account for the combined effects of heat and humidity, the National Weather Service (NWS) has adopted the Heat Index, which attempts to calculate the apparent “felt” temperature by adjusting for humidity. Table 4 summarizes hazards associated with high values of the Heat Index (NWS 2013).

NWS calculates the Heat Index only when air temperature is greater than or equal to 80 °F and relative humidity is greater than or equal to 40 percent. Heat Index values are summarized graphically in Figure 10, which shows how the combined impact of humidity and temperature create dangerous conditions. The values shown in this chart are derived from the mathematical formula given in Appendix A.

Table 4. Interpretation of the Heat Index (NWS 2013)

Celsius	Fahrenheit	Notes
27–32 °C	80–90 °F	Caution: fatigue is possible with prolonged exposure and activity. Continuing activity could result in heat cramps.
32–41 °C	90–105 °F	Extreme caution: heat cramps and heat exhaustion are possible. Continuing activity could result in heat stroke.
41–54 °C	105–130 °F	Danger: heat cramps and heat exhaustion are likely; heat stroke is probable with continued activity.
Over 54 °C	Over 130 °F	Extreme danger: heat stroke is imminent.

Note: Exposure to direct sunlight can increase the Heat Index by up to 8 °F.

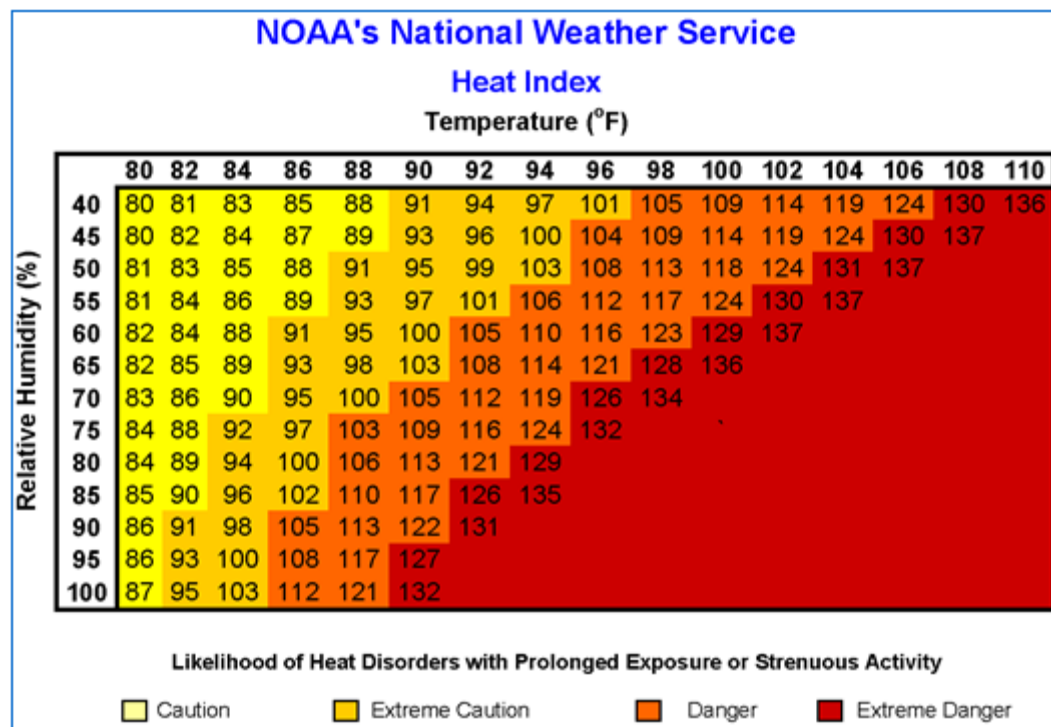


Figure 10. NWS Heat Index chart including hazard zones (NWS 2013).

The existing climate series developed for *SafeWater* RI included temperature and dew point from the Providence Airport station (COOP ID RI376698) but not relative humidity. Therefore, relative humidity was estimated from temperature and dew point using the August-Roche-Magnus approximation, as outlined in Appendix B.

This approach is considered valid for air temperatures between 32 to 140 °F (0 and 60 °C) and dew point temperatures between 32 to 122 °F (0 and 50°C). For cases where the approximation resulted in relative humidity slightly greater than 100 percent, relative humidity was capped at 100 percent.

The BCSD GCM archives do not provide estimates of future dew point temperature or relative humidity. However, Tetra Tech had previously developed monthly dew point change statistics for 2052 for the weather station at Franklin, Massachusetts (MA192997), just a few miles north of the Rhode Island border (USEPA 2013a). These change statistics come from climate products that were dynamically downscaled using regional climate models (RCMs) as part of the North American Regional Climate Change Assessment Program (NARCCAP; <http://www.narccap.ucar.edu>). Since this station is only one NARCCAP grid-cell removed from Providence, Rhode Island, it was assumed to provide a reasonable estimate of the relative changes in dew point that Rhode Island might experience.

The NARCCAP scenarios cover only a subset of the BCSD scenarios because of the cost and effort of running RCMs coupled to GCMs. At the time of the analysis, the RCM-GCM model pairs available were CRCM-CGCM3, HRM3-HADCM3, RCM3-GFDL, GFDLhighres-GFDL, RCM3-CGCM3, and WRFG-CCSM, all developed for the A2 scenario. It was assumed that the same change statistics applied for dew point but not temperature under the A2 and B1 scenarios, and the NARCCAP average results were used and provided more than one downscaled product for a GCM (relevant to GFDL and CGCM3 models).

The monthly dew point change statistics were then applied to the baseline dew point temperature time series from the Providence Airport station to develop dew point temperature time series for each of the

eight scenarios for time horizon 2052. The previously developed temperature time series for the eight climate scenarios in 2052 were then combined with the corresponding 2052 dew point temperature series to develop relative humidity and Heat Index time series at T_{max} separately for each scenario using the formulas outlined above.

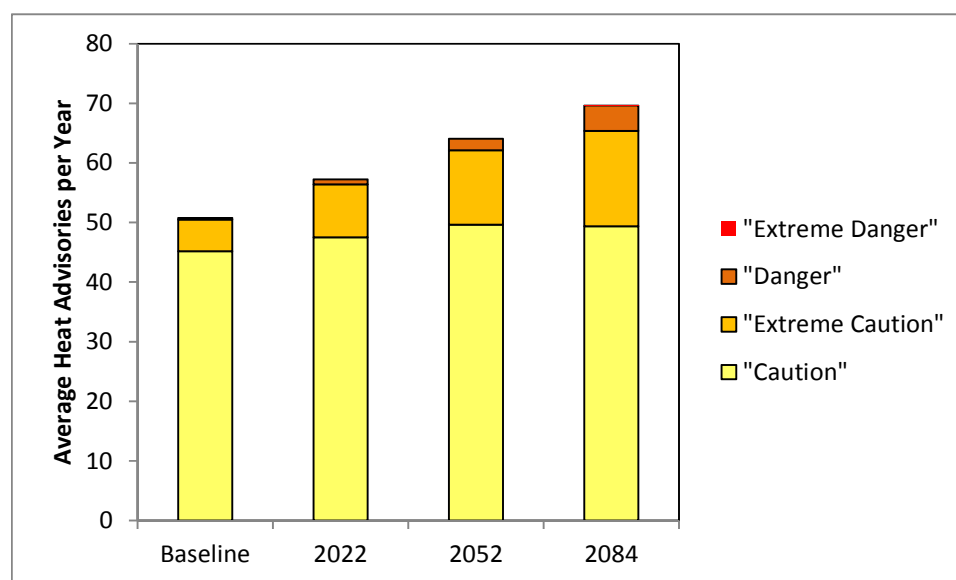
Dew point change statistics from the prior work are available for only 2052, so further assumptions were necessary to develop Heat Index time series for 2022 and 2084. The main assumption is that the same relative humidity, but not the actual dew point, applies to the 2022 and 2084 scenarios as in the 2052 scenario. Thus, the relative humidity time series calculated for each of the eight climate scenarios in 2052 was applied to 2022 and 2084 and combined with the air temperature projections for those time periods to calculate the Heat Index.

Results are summarized in terms of the average number of heat advisories per year based on 30 years of simulated data. Table 5 documents results by scenario, and Figure 11 provides a summary of the central tendency, averaged across all scenarios. This shows a gradual projected increase in the number of heat advisories, from 51 per year under baseline conditions to 70 per year under 2084 conditions. Likely of greater concern, the number in the “Danger” and “Extreme Danger” categories is projected to increase from near zero (0.3 and 0 per year, respectively) to 4.3 and 0.13 per year. The counts of “Extreme Danger” remain relatively low because the highest temperatures are projected to occur with moderate humidity (e.g., air temperature of 108.7 °F, coupled with relative humidity of 35 percent, yields a Heat Index of 125.7).

It is worth noting that the baseline (1978–2007) on which the future time series are built does not include the heat wave of July 2010. On July 6, 2010, a new record temperature of 102 °F was set at Providence Airport, with a Heat Index of 120 (in the “Danger” range). If this period had been included in the baseline time series, a slightly higher count of average annual heat advisories would have been estimated for all time horizons.

Table 5. Average Number of Heat Advisories per Year by Model Scenario for Current, 2022, 2052, and 2084 Time Horizons

Scenario	Model	"Caution"	"Extreme Caution"	"Danger"	"Extreme Danger"	Total Heat Advisories
Baseline	Baseline	45.2	5.3	0.3	0.0	50.8
2022_W1	CGCM3_A2	48.9	8.7	0.8	0.0	58.4
2022_W2	CGCM3_B1	45.1	9.0	0.9	0.0	55.0
2022_W3	GFDL_A2	50.4	9.5	0.8	0.0	60.7
2022_W4	GFDL_B1	48.5	9.8	0.9	0.0	59.1
2022_W5	CCSM_A2	49.3	8.1	0.7	0.0	58.0
2022_W6	CCSM_B1	46.5	9.2	0.9	0.0	56.6
2022_W7	HadCM3_A2	46.9	8.3	0.8	0.0	56.0
2022_W8	HadCM3_B1	44.9	8.5	0.8	0.0	54.2
2052_W1	CGCM3_A2	49.3	12.6	1.9	0.0	63.9
2052_W2	CGCM3_B1	47.4	11.1	1.6	0.0	60.2
2052_W3	GFDL_A2	52.3	13.9	2.3	0.0	68.5
2052_W4	GFDL_B1	50.5	12.7	2.0	0.0	65.2
2052_W5	CCSM_A2	52.2	12.4	1.8	0.0	66.4
2052_W6	CCSM_B1	47.9	10.5	1.2	0.0	59.6
2052_W7	HadCM3_A2	49.3	13.8	2.5	0.0	65.7
2052_W8	HadCM3_B1	48.4	12.4	2.1	0.0	62.9
2084_W1	CGCM3_A2	51.0	18.3	5.7	0.2	75.1
2084_W2	CGCM3_B1	47.0	13.5	2.3	0.0	62.8
2084_W3	GFDL_A2	51.5	19.7	6.8	0.3	78.2
2084_W4	GFDL_B1	51.6	13.8	2.2	0.0	67.6
2084_W5	CCSM_A2	53.4	17.8	4.4	0.1	75.6
2084_W6	CCSM_B1	48.0	10.7	1.4	0.0	60.1
2084_W7	HadCM3_A2	46.8	18.5	7.5	0.5	73.3
2084_W8	HadCM3_B1	46.1	15.6	3.9	0.1	65.6

**Figure 11. Heat advisories per year, averaged across all scenarios.**

4 Heat Variability

Extreme heat can cause many heat-related illnesses in humans, from mild heat rash to deadly heat stroke. Prolonged heat exposure can also exacerbate several chronic diseases, including cardiovascular and respiratory disease. The simple evaluation of health risks associated with rising temperature in terms of Heat Index explained in Section 3 misses an important subtlety, the additional heat-related risk factors associated with potential changes in the *variability* of heat.

Large temperature fluctuations have been shown to have a greater effect on health risks than sustained high temperatures, which allow for adaptation. This is explained in research reported by Zanobetti et al. (2012), which shows that the variability of summer temperatures has an important influence on health outcomes, particularly among the elderly.

The variability in summer (June–August) temperatures may be summarized through the standard deviation (*SD*), which is the square root of the mean of the squared differences between the temperature on a given day and the average temperature for the summer period. For normally distributed data, about 95 percent of individual observations will lie within two standard deviations of the mean. Zanobetti et al. (2012) conducted a nationwide (135-city) study to investigate the relationship between summer temperature standard deviation (*SD*) and health outcomes in elderly populations. The researchers reported results for four at-risk populations: persons with chronic obstructive pulmonary disease (COPD), persons with congestive heart failure (CHF), persons with diabetes, and persons with myocardial infarction (MI). The study estimated hazard ratios (HR), which are calculated as the relative change in mortality for every 1 degree Celsius increase in summer temperature *SD*, summarized by climate zone. Table 6 presents the study findings.

Except in the coldest climate zone (i.e., northern New England – zone 1), there is an increase in HR for all the defined at-risk populations with increased summer temperature *SD*. Rhode Island falls into climate zone 2. Therefore, increased mortality would be expected in all these at-risk populations if summer temperature *SD* increases.

Predicting future summer temperature *SD* is difficult because the ability of climate models to predict variability in weather at the daily scale is uncertain. There are two potential contributors to increased *SD*. The first is simply a scale effect. That is, if the average summer temperature increases and the relative magnitude of day-to-day temperature variability remains unchanged, then *SD* will also increase. The second potential contributor is an actual change in the pattern of variability.

Table 6. Hazard Ratio for a 1 °C Increase in Yearly Summer Temperature *SD* by Climate Region

Climate Zone	Hazard Ratio (<i>HR</i>)				
	CHF	MI	Diabetes	COPD	Average
1 (coldest)	0.997	0.984	0.998	1.015	0.999
2	1.013	1.020	1.020	1.019	1.018
3	1.020	1.030	1.022	1.021	1.023
4	1.042	1.051	1.052	1.047	1.048
5 (hottest)	1.057	1.095	1.098	1.078	1.082

Source: Zanobetti 2012.

The projected future climate time series created for watershed modeling and described in Section 2.1 are poorly suited to investigate this issue. Specifically, the future temperature time series are created by modifying historical records by adding a delta change factor. Adding a constant to a set of data does not change the *SD*. Thus, examination of the *SD* of summer temperature in the climate scenario time series reveals only a small change in *SD*. (The small change that does occur, with a maximum increase of 0.5 °F [0.28 °C], is a result of differences in the delta value between months.)

Given that it is likely not appropriate to infer changes in summer temperature *SD* from the time series modified by the delta change method, additional information might be extracted from the raw climate model output. The BCSD products used in this project are, however, at monthly scale only.⁴ The standard deviation of summer *monthly* average temperature in the BCSD data set does increase, with a median increase of 0.11 °C in *SD* by 2084 and a maximum increase of 0.92 °F (0.51 °C) (GFDL A2, 2084). Assuming a linear increase in HR from a temperature change of 0 to 1 °C, the average HR under an increase in summer *SD* of 0.11 °C would be 1.002. That, corresponding to an increase in summer *SD* of 0.51, would be 1.009. (In other words, the mortality rate for a given disease would increase by 9 persons for every 1,000 deaths under current conditions.) The actual effect might be larger, but determining the effect would require daily data directly from the climate model for analysis.

To better understand the scope of heat exposure, mortality data for 1999–2009 were used to review heat-related deaths in the United States overall. During this period, 7,233 heat-related deaths occurred, an average of 658 per year. In Rhode Island there have been 19 heat-related deaths during 1999–2013 (for both underlying and contributing causes). Nine were female and ten were male.

Early research performed by HEALTH in coordination with Brown University shows that...

The different climate scenarios chosen for this study reveal an increase in warm days for each time horizon modeled. The number of days in a year between 70 and 80 degrees F increase with which time horizon for nearly all scenarios at varying rates.

Average number of days per year that are 70-80°F (21.10-26.67°C)

Time Horizon	Baseline	W1	W2	W3	W4	W5	W6	W7	W8
2022	48	57	55	60	59	57	57	56	54
2052	48	64	60	63	63	65	61	64	64
2084	48	65	64	60	64	67	61	59	64

Average number of days per year that are 70-80°F (21.10-26.67°C)

Time Horizon	Baseline	W1	W2	W3	W4	W5	W6	W7	W8
2022	13%	16%	15%	16%	16%	16%	16%	15%	15%
2052	13%	18%	17%	17%	17%	18%	17%	17%	17%
2084	13%	18%	17%	16%	18%	18%	17%	16%	17%

⁴ A companion BCCA daily bias-corrected product is now available for a subset of climate models, but it was not available when this report was written.

5 Pollen and Allergens

Intensification of allergen-related illness is another potential health impact of warmer air temperatures. Warmer temperatures will mean earlier blooms and later frosts, which will lengthen allergy season. Allergic diseases, such as asthma and allergic rhinitis, have a complex etiology but are exacerbated by exposure to airborne allergens (or aeroallergens). Concentrations of natural aeroallergens, predominantly plant pollen and mold spores, are an important health risk factor for sensitive individuals and are expected to be sensitive to changes in climate (USEPA 2008b). This section focuses on potential changes in airborne pollen, although mold spores are also likely to increase under warmer and wetter conditions.

Pollen production is associated with flowering of plants. There are two major strategies for the timing of plant flowering and two general types of associated climate impacts. First, many trees, including key aeroallergen producers such as birch, time their flowering based on warming temperatures in spring. It is predicted that the dates of both start and peak dates of birch pollen production will be 2 to 4 weeks earlier in the year 2100 than in the year 2000, and that pollen production rates will increase from 1.3 to 8 times, due to the combined effects of increased carbon dioxide (CO₂) concentrations and warmer spring temperatures (Zhang et al. 2013). The second flowering strategy used by most summer annuals (including major aeroallergen producers such as ragweed) initiates flowering based on a minimum day length. For many of these plants, flowering will continue until first frost. Thus, later dates of first frost will extend the pollen season. Ziska et al. (2011) estimated that later frost has resulted in an increase in the length of the ragweed pollen season by 12 to 27 days at latitudes above ~44° N since 1995 (Augusta, Maine, is located along 44° N). Continued warming might also result in significantly greater exposure times to seasonal allergens, with subsequent effects on public health.

The Soil and Water Assessment Tool (SWAT) model developed for analysis of watershed response to climate change (Tetra Tech 2013) includes an integrated plant growth model. This can help evaluate changes in the onset of the spring pollen season. In addition, the predicted first fall frost is available from the input time series assembled for the SWAT model. Both aspects are subject to uncertainty. For the start of tree bloom, SWAT has a generic assumption that this is timed to 15 percent of the total annual heat units (relative to a base of °C), as calculated based on weather station statistics for 1970–2000. The start of bloom timing (which works out to a median of May 3 for simulation of the 1978–2007 baseline data) has not been verified against the actual bloom start data for Rhode Island. The date of first frost incorporates climate model predictions about changes in monthly average temperature, but it does not account for systematic changes in extreme weather (such as the timing of Canadian cold fronts) that may have important influences on plant kill dates. Furthermore, the analysis does not take into account the differential sensitivity of allergen-producing plants to subfreezing temperatures. Some allergen-producing plants die at daily minimum temperatures below freezing, while others have some resistance to temperatures several degrees lower.

Given these uncertainties, the best use of existing models is to explore the *relative* changes in the predicted length of the aeroallergen production season. (As noted above, reliable tools to predict changes in aeroallergen intensity were not available.) Different GCMs produce different results. (See Figure 12 for details of individual GCM scenarios compared to present-day (1978–2007) conditions.) However, all the climate models agree that spring bloom is likely to occur somewhat earlier (median of 21 days earlier by 2084) and first frost later (median of 17 days later by 2084). An earlier bloom and later frost will contribute to a greater length of the aeroallergen season, as shown in Figure 12. In this figure, the different climate scenarios differ considerably in the date of onset of plant growth and date of first frost; however, all models predict an earlier onset of growth and a delay in first frost. Table 7 summarizes median results across all climate scenarios. These suggest that by 2084 spring bloom may occur about 3

weeks earlier and fall frost about 17 days later, for a median net increase in the length of the aeroallergen season of 37 days.⁵

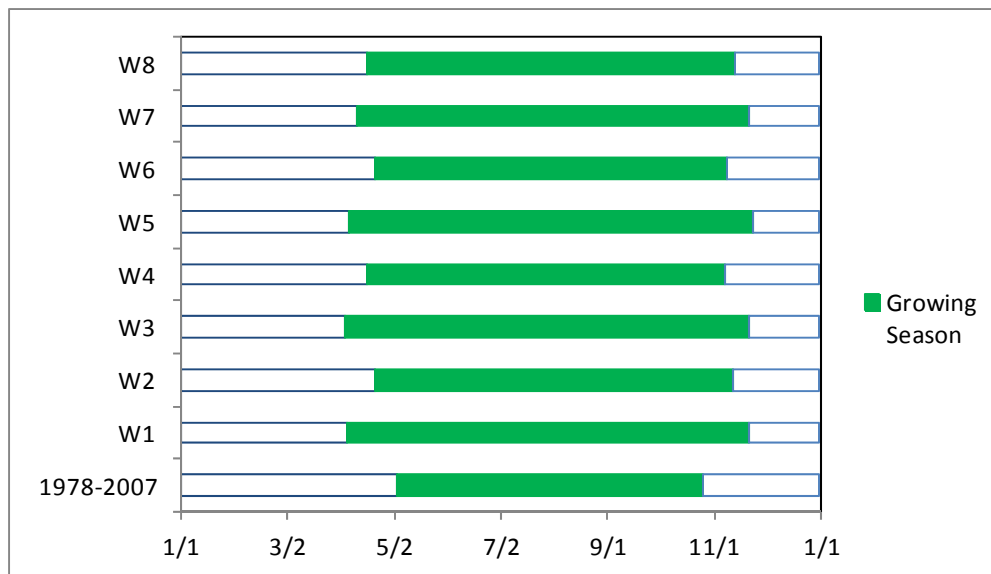


Figure 12. Length of growing season predicted by SWAT for the 1978–2007 baseline and eight climate change scenarios centered at 2084.

Note: The growing season shown is defined as the period from the onset of spring tree growth (defined as 15 percent of the base-zero potential heat units defined on 1970–2000 climatology) and first frost. Each horizontal category (i.e., W1, W2, W3, etc.) corresponds to a climate change scenario described in Section 2.1.

Table 7. Length of Aeroallergen Production Season, Median of Climate Model Projections

Time horizon	Tree bloom	First freeze	Season length
1978–2007 baseline	May 3	October 25	177
2022	April 27	November 3	190
2052	April 20	November 9	203
2084	April 12	November 12	214

⁵ The pollen projections are based on Rhode Island specific temperature and growing season projections. However, this assessment does not use pollen production or start of bloom dates specific to Rhode Island.

6 Disease Vectors and Climate

A changing climate will alter physical and ecological conditions for a variety of disease-carrying insects and parasites. Although the full ramifications for many diseases are not well understood, this section focuses on two of the better-studied examples relevant to Rhode Island.

In the northeastern United States, two of the most significant disease vectors are mosquitoes that convey West Nile Virus (WNV) and ticks that transmit Lyme disease (Frumhoff 2007). In addition to Lyme disease and West Nile Virus, there are other vector-borne diseases that have been found in Rhode Island, including Eastern Equine Encephalitis, Malaria, Babesiosis, Ehrlichiosis, and Rocky Mountain Spotted Fever. Ticks and mosquitoes are sensitive to physical conditions, such as humidity, daily high and low temperatures, rainfall patterns, and winter snowpack. Temperature and precipitation have been shown to influence mosquito and tick populations, and these climate indicators can be used to create projections of future disease incidence.

6.1 TICKS AND LYME DISEASE

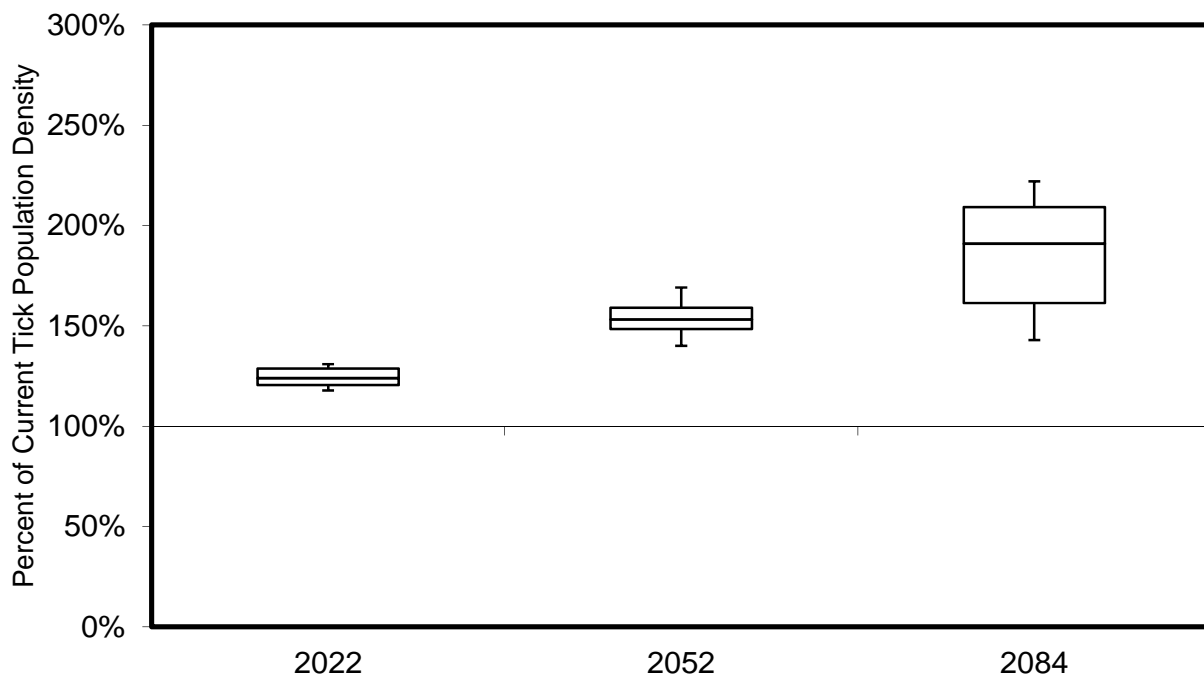
Lyme disease is caused by a bacterial organism that is transmitted to humans via the bite of an infected tick. The first stage of Lyme disease may begin with a bull's-eye rash and flu-like symptoms such as fever, chills, swollen lymph nodes, headaches, fatigue, muscle aches, and joint pain. Later symptoms can include neurological complications such as numbness, pain, weakness, Bell's palsy (paralysis of the facial muscles), visual disturbances, memory loss, sleep disorder, meningitis, and many other conditions (NINDS 2013).

Most humans are infected through the bites of immature ticks called nymphs. Nymphs are tiny (less than 2 mm) and difficult to see; they feed during the spring and summer months. Adult ticks can also transmit Lyme disease bacteria, but they are much larger and may be more likely to be discovered and removed before they have had time to transmit the bacteria. Adult ticks are most active during the cooler months of the year. As the prevailing weather and climate conditions change into the future, the abundance and range of ticks, especially those in the nymph stage, will likely increase throughout the Northeast. Data collected by the University of Rhode Island's (URI) Center for Vector-Borne Disease showed that the tick population in 2012 was 80 percent higher than the 2011 population estimates (TickEncounter Resource Center 2012). If humidity and temperature continue to increase during the spring, summer, and fall, this trend may continue. As explained in the following paragraphs, statistical analyses of tick populations predict that the average annual tick population near the end of the century could be nearly double what it is today. This increase is likely to result in an increase in tick bites, creating a corresponding increase in the risk of contracting Lyme disease.

While year-to-year variability in tick population is related to humidity, the general trend in tick populations is believed to be strongly influenced by air temperature, with higher temperatures and longer frost-free periods leading to more ticks. Ogden (2004) discusses the effects of climate on populations of deer ticks (*Ixodes scapularis*; also called blacklegged ticks), which are a major vector species for Lyme disease (CDC 2013). Ogden describes a relationship between the mean annual degree days in a year and the number of feeding adult ticks in a given region. Although the size of the tick population is not a direct indicator of Lyme disease incidence, the projected tick population does provide a basis for comparison of relative risk between climate scenarios. The research is based on study areas in Quebec and Ontario, Canada, and established a linear relationship between tick population and mean annual degree days (°C) with an average slope of 0.464. The regression analysis showed a strong association between the maximum number of ticks and the mean annual number of degree-days greater than 0°C.

Degree days are simply the sum of daily temperatures greater than 0 °C over the course of a year, and they are otherwise referred to as potential heat units relative to zero (PHU₀). They were calculated from the 30-year time series of climate data created for each climate scenario (Section 2.1). The linear regression equation (representing the average values) presented in Table 6 was then used to estimate the future tick population in each year and across each of the 24 climate scenarios. The yearly results were then averaged to generate the average tick population change for each scenario. The ratio of average tick population under future climate to that under existing climate provides an approximate indicator of changes in Lyme disease risk and is presented in Figure 13 by means of boxplots. In this figure, the box shows the interquartile range (25th percentile to 75th percentile), with the median indicated by a horizontal line. The whiskers extend 1.5 times the interquartile range and provide a nonparametric estimate of 95 percent confidence intervals on the median. The figure shows a continuing increase in risk, predicting that the average annual tick population in 2084 could be nearly double (191 percent) that of today. This increase in tick population is likely to result in an increase in human tick bites and a corresponding increase in the risk of contracting Lyme disease.

Research compiled by Dr. Thomas Mather⁶ shows that nymphal deer tick abundance and disease rates are determined by relative humidity levels in June; higher humidity means greater tick survival, more tick encounters, and more disease. Episodes of low humidity (below 80%), even as brief as 8 to 10 hours, will cause nymphal deer ticks to dry out and die earlier in the tick season. The available climate model output used in this study has projected future relative humidity for only 2052 conditions. The models suggest that changes in June relative humidity will be small, with the average relative humidity at the hottest time of the day increasing from 51.7 percent to 53.2 percent, indicating there will not be increased dryness that would help mitigate the tick problem. It thus appears that the increases in temperature will provide an ideal summer climate for ticks to flourish.



⁶ University of Rhode Island (URI), Center for Vector-Borne Disease.

Figure 13. Predicted density of deer tick population in Rhode Island relative to current climate conditions.

6.2 MOSQUITOES AND WEST NILE VIRUS

Under current conditions in Rhode Island, mosquitoes can transmit both West Nile Virus and Eastern Equine Encephalitis (EEE) Virus (Ginsberg et al. 2013). A number of other major diseases, such as dengue fever, yellow fever, and malaria, are transmitted by mosquitoes in more tropical climates, but they are rarely found in the northeastern United States, primarily because of the environmental requirements of their host mosquito species (Gubler et al. 2001; Reiter 2001). For instance, yellow fever and dengue fever occur only where temperatures rarely fall below 50 °F—a constraint that will remain in place for Rhode Island throughout the 21st century. This report studies the impacts a changing climate might have on the incidence of West Nile Virus only because EEE is a rare illness most cases of which occur in the Atlantic and Gulf Coast states.

West Nile Virus is a flavivirus commonly found in Africa, West Asia, and the Middle East. How long it has been in the United States is not known, but CDC scientists believe the virus has probably been in the eastern United States since the early summer of 1999, possibly longer. Mosquitoes become infected when they feed on infected birds, which may circulate the virus in their blood for a few days. Infected mosquitoes can then transmit West Nile virus to humans and animals when they bite. Anyone can get infected with the West Nile Virus; however the risk of getting sick is low for most of the population. Individuals with certain medical conditions, such as cancer, diabetes, high blood pressure, and kidney disease are at greater risk for serious illness if infected with West Nile Virus.

Symptoms of severe West Nile Virus illness can include high fever, headache, neck stiffness, stupor, disorientation, coma, tremors, convulsions, muscle weakness, vision loss, numbness and paralysis. These symptoms may last several weeks, and neurological effects may be permanent. Up to 20 percent of the people who become infected have milder symptoms such as fever, headache, and body aches, nausea, vomiting, and sometimes swollen lymph glands or a skin rash on the chest, stomach and back. Milder symptoms can last for as short as a few days, though even healthy people have become sick for several weeks. Approximately 80 percent of people (about 4 out of 5) who are infected with WNV will not show any symptoms at all.

Prediction of the incidence of mosquito-borne disease in response to climate is difficult because there are many complex interacting factors. Different diseases are transmitted by different mosquito species, each of which has different environmental requirements. A wetter climate will generally increase risk because mosquitoes lay their eggs in standing water. Temperature effects are complex. As noted above, temperature may limit the range of host species; however, hotter weather also limits the mosquitoes' life span but increases their biting speed (Hartley et al. 2012). In the case of West Nile Virus, hotter temperatures also increase the rate at which the virus gets into the mosquito salivary glands and becomes transmittable (Kilpatrick et al. 2008). Even animal behavioral responses to climate, such as changes in migration timing by bird species, may have an important impact. For instance, West Nile Virus epidemics have been associated with the timing of the dispersal of robins (the preferred avian host for the mosquito vector; Kilpatrick et al. 2006).

West Nile Virus transmission is now relatively well understood and is presented as an example of potential climate impacts on mosquito-borne pathogens in general. Ruiz et al. (2010) present a relationship between temperature, precipitation, and West Nile Virus infection in *Culex* species mosquitoes. The researchers fit four linear regression models for West Nile Virus infection rates. Two of the models involve autoregressive terms and are most appropriate for step-ahead forecasting. This report uses Ruiz et al.'s (2010) model 2, which had the best fit of the models without autoregressive terms ($R^2 = 0.70$):

$$MIR = 0.35 \text{ prcp3wk} - 1.57 \text{ prcp_annual} + 0.42 \text{ DW},$$

in which *MIR* is the minimum infection ratio for the week (the ratio of the number of mosquitoes that carry West Nile Virus to the total number of mosquitos in each pooled sample, expressed as a percentage), *prcp3wk* is the 3-week average precipitation calculated up to 3 weeks prior to the current week, *prcp_annual* is the annual precipitation from the prior year, and *DW* is the accumulated degree weeks for the preceding week relative to a base temperature of 22 °C.

There are some uncertainties and confusion as to units in the Ruiz et al. (2010) study, but this report has provided what is believe to be the correct interpretation. The model was evaluated for each week over the 30-year simulation period. Figure 14 shows example results for the baseline simulation of year 2008. To compare between scenarios, average MIR was calculated for weeks 27 through 39 in July through September. (The declining period that occurs after average weekly temperature falls below 22 °C is omitted from the averages because it involves an autoregressive term.)

Projected MIRs for West Nile Virus under future climate conditions are shown in Table 8 and summarized graphically in Figure 15. All scenarios project significant increases in the West Nile Virus infection rate. The median MIR value increases nearly four-fold by the 2084 time horizon, suggesting that significant effort may be required to protect public health. It should be noted that since all scenarios project increases in West Nile Virus infection, it is possible that infection rates for Eastern Equine Encephalitis could also increase because the virus has been confirmed in multiple mosquito traps tested by the state.

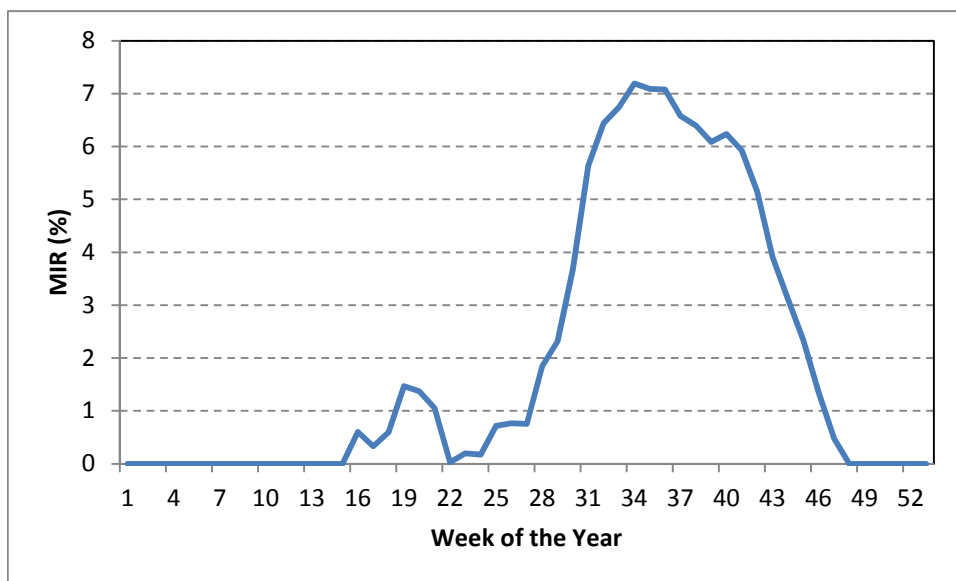


Figure 14. Example minimum infection ratio (MIR) for West Nile Virus in *Culex* mosquitoes, baseline simulation for 2008.

Note: MIR is an estimate of the fraction of the mosquito population that carries West Nile Virus.

Table 8. Projected Minimum Infection Ratio (MIR, %) for West Nile Virus in *Culex* Mosquitoes under Baseline and Future Climate Scenarios W1–W8 (July–September Average)

	W1	W2	W3	W4	W5	W6	W7	W8	Median
Baseline	3.5	3.5	3.5	3.5	3.5	3.5	3.5	3.5	3.5
2022	5.5	5.5	7.2	6.7	5.3	5.5	5.1	5.1	5.5
2052	8.7	6.9	10.8	9.3	8.6	6.7	9.7	8.1	8.6
2084	15.6	8.8	18.3	10.2	14.5	6.7	17.8	11.6	13.0

Note: MIR is an estimate of the fraction of the mosquito population that carries West Nile Virus.

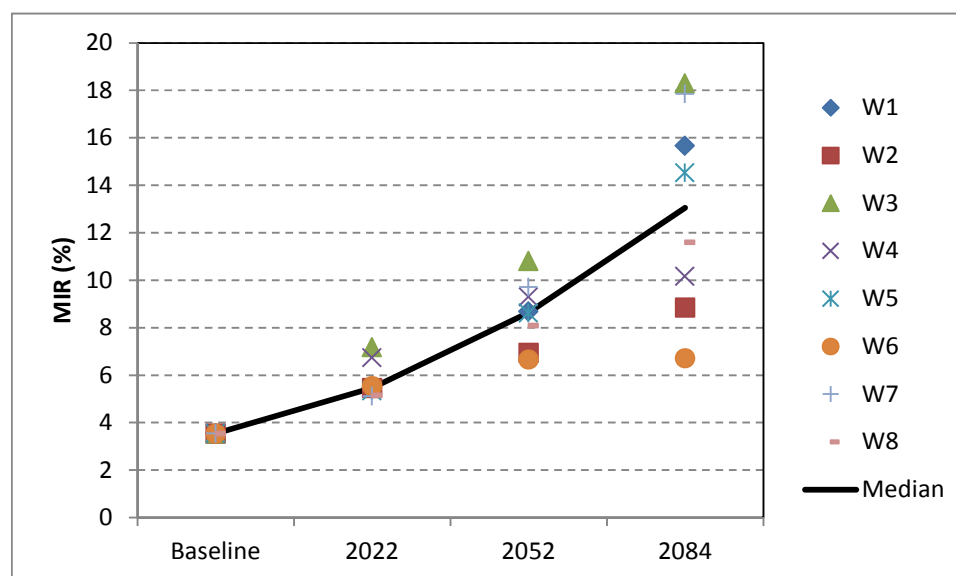


Figure 15. Projected time course of minimum infection ratio (MIR) for West Nile Virus in *Culex* Mosquitoes under Baseline and Future Climate Scenarios (July–September Average)

Note: MIR is an estimate of the fraction of the mosquito population that carries West Nile Virus.

(This page left intentionally blank.)

7 Conclusions

The preliminary analyses presented in this report suggest that Rhode Island residents are likely to face increased health risks from climate-related hazards over the coming decades, including extreme heat advisories, extended allergy seasons, and increased incidence of Lyme disease and West Nile Virus. The heat and humidity assessment shows that the number of days in the “Danger” category, when heat cramps and heat exhaustion are likely, is projected to increase from near zero to 4.3 days per year through 2084. Similarly, the number of days in the “Extreme Danger” category, when heat stroke is imminent, is projected to increase from zero days under baseline conditions to 0.13 days per year through 2084.

Additionally, all the climate projections suggest earlier spring blooms and later first frosts in fall, resulting in a lengthening of the allergy season in Rhode Island. This will exacerbate and increase the duration of symptoms in individuals with allergic diseases, such as asthma and allergic rhinitis.

As temperatures rise, rainfall and humidity patterns change, and summers become longer, ticks and mosquitos will remain active for longer periods of time and inhabit more regions across the United States. The climate models and tick prevalence data indicate that the tick population will continue to grow through mid-century and nearly double in size by 2084 compared to current average conditions. The infectiousness of mosquitoes for West Nile Virus is also likely to increase, and mosquito-borne diseases such as Equine Encephalitis Virus could also increase. Additional strategies will need to be deployed to prevent increases in such diseases.

It is important to note that the results of this report are only preliminary estimates of future trends, and the possible range of outcomes that might require adaptation. Rhode Island must continue to monitor climate changes to further understand immediate and future impacts. The human health impacts discussed in this report will require that Rhode Island develop adaptation strategies geared toward protecting its citizens’ health into the future.

(This page left intentionally blank.)

8 References

- Anandhi, A., A. Frei, D.C. Pierson, E.M. Schneiderman, M.S. Zion, D. Lounsbury, and A.H. Matonse. 2011. Examination of change factor methodologies for climate change impact assessment. *Water Resources Research*, 47: doi:10.1029/2010WR009104.
- CDC (Centers for Disease Control and Prevention). 2013. Lyme Disease Transmission.
- Dai, A. 2006. Precipitation characteristics in eighteen coupled climate models. *Journal of Climate*, 19:4605–4630.
- Frumhoff, Peter. 2007. Confronting Climate Change in the U.S. Northeast. Northeast Climate Impacts Assessment.
- Ginsberg, H.S., A. Gettman, E. Becker, A.S. Bandyopadhyay, and R.A. Lebrun. 2013. Environmental management of mosquito-borne viruses in Rhode Island. *Rhode Island Medical Journal*, 96(7):33–35.
- Gubler, D.J., P. Reiter, K.L. Ebi, W. Yap, R. Nasci, and J.A. Patz. 2001. Climate variability and change in the United States: Potential impacts on vector and rodent-borne diseases. *Environmental Health Perspectives*, 109(Supplement 2):223–233.
- Hartley, D.M., C.M. Barker, A. Le Menach, T. Niu, H.D. Gaff, and W.K. Reisen. 2012. Effects of temperature on emergence and seasonality of West Nile virus in California. *American Journal of Tropical Medicine and Hygiene*, 86 (2012): 884–894.
- IPCC (Intergovernmental Panel on Climate Change). 2007. Climate Change 2007: Synthesis Report—Summary for Policymakers. Available online at: http://www.ipcc.ch/pdf/assessment-report/ar4/syr/ar4_syr_spm.pdf.
- Karl, T.R., J.M. Melillo, and T.C. Peterson, eds. 2009. *Global Climate Change Impacts in the United States*. Cambridge, UK: Cambridge University Press.
- Kilpatrick, A.M., L.D. Kramer, M.J. Jones, P.P. Marra, and P. Daszak. 2006. West Nile virus epidemics in North America are driven by shifts in mosquito feeding behavior. *PLOS Biology*, 4(4): e82.
- Kilpatrick, A.M., M.A. Meola, R.M. Moudy, and L.D. Kramer. 2008. Temperature, viral genetics, and the transmission of West Nile virus by *Culex pipiens* mosquitoes. *PLOS Pathogens*, 4(6): e1000092.
- Nakicenovic, N., J. Alcamo, G. Davis, B. de Vries, J. Fenhann, S., K. Gregory, A. Grübler, T. Y. Jung, T. Kram, E. L. La Rovere, L. Michaelis, S. Mori, T. Morita, W. Pepper, H. Pitcher, L. Price, K. Riahi, A. Roehrl, H.-H. Rogner, A. Sankovski, M. Schlesinger, P. Shukla, S. Smith, R. Swart, S. Van Rooijen, N. Victor, and Z. Dadi. 2000. *Special Report on Emissions Scenarios*. A Special Report of Working Group III of the Intergovernmental Panel on Climate Change published for the Intergovernmental Panel on Climate Change. Cambridge, UK: Cambridge University Press. Available online at: www.ipcc.ch/pdf/special-reports/emissions_scenarios.pdf.
- National Institute of Neurological Disorders and Stroke (NINDS). 2013. NINDS Neurological Complications of Lyme Disease Information Page. *National Institutes of Health*. Available online at: www.ninds.nih.gov/disorders/lyme/lyme.htm.
- National Weather Service. 2013. The National Oceanic and Atmospheric Administration's Watch, Warning, and Advisory Products for Extreme Heat. National Oceanic and Atmospheric

- Administration (NOAA) National Weather Service, Office of Climate, Water, and Weather Services. Available online at: <http://www.nws.noaa.gov/os/heat/index.shtml>.
- Ogden, N.H. 2004. A dynamic population model to investigate effects of climate on geographic range and seasonality of the tick *Ixodes scapularis*. *International Journal of Parasitology*, 35: 375–389.
- Reiter, P. 2001. Climate change and mosquito-borne diseases. *Environmental Health Perspectives*, 109 (Supplement 1): 141–161.
- Ruiz, M.O., L.F. Chaves, G.L. Hamer, T. Sun, W.M. Brown, E.D. Walker, L. Haramis, T.L. Goldberg, and U.D. Kitron. 2010. Local impact of temperature and precipitation on West Nile virus infection in *Culex* species in northeast Illinois, USA. *Parasites and Vectors*, 3:19.
- Spronken-Smith, R., and T. Oke. 1998. The thermal regime of two parks in two cities with different summer climates. *International Journal of Remote Sensing*, 19(1): 2085–2104.
- Sun, Y., S. Solomon, A. Dai, and R.W. Portmann. 2006. How often does it rain? *Journal of Climate*, 19:916–934.
- Tetra Tech. 2012. SafeWater RI: Phase 2 Report, Assessment of Impacts. Prepared for Rhode Island Department of Health, Office of Drinking Water Quality by Tetra Tech, Inc., Fairfax, VA.
- TickEncounter Resource Center. 2012. URI entomologist says deer tick numbers are up significantly statewide, increasing risk of contracting Lyme disease. University of Rhode Island Center for Vector-Borne Disease and TickEncounter Resource Center. Available online at: www.tickencounter.org/news/latest_efforts_to_combat_lyme_disease.
- USEPA (U.S. Environmental Protection Agency). 2008a. *Reducing Urban Heat Islands: Compendium of Strategies*. State and Local Climate and Energy Program, Washington, DC. Available online at <http://www.epa.gov/hiri/resources/compendium.htm>.
- USEPA (U.S. Environmental Protection Agency). 2008b. *Review of the Impacts of Climate Variability and Change on Aeroallergens and Their Associated Effects*. National Center for Environmental Assessment, Office of Research and Development, Washington, DC. EPA/600/R-06/164F.
- USEPA (U.S. Environmental Protection Agency). 2009. *ICLUS V1.2 User's Manual: ArcGIS Tools and Datasets for Modeling US Housing Density Growth*. Global Change Research Program, National Center for Environmental Assessment, Office of Research and Development, Washington, DC. EPA-600-R-09-143A.
- USEPA (U.S. Environmental Protection Agency). 2013a. *Watershed Modeling to Assess the Sensitivity of Streamflow, Nutrient, and Sediment Loads to Potential Climate Change and Urban Development in 20 U.S. Watersheds*. National Center for Environmental Assessment, Washington, DC. EPA/600/R-12/058F. Available from the National Technical Information Service, Springfield, VA, and online at <http://www.epa.gov/ncea>.
- USEPA (U.S. Environmental Protection Agency). 2013b. *Integrated Climate and Land Use Scenarios (ICLUS)*. Global Change Research Program website. Available online at: <http://www.epa.gov/ncea/global/iclus/>.
- Zanobetti, A., M.S. O'Neill, C.J. Gronlund, and J.D. Schwartz. 2012. Summer temperature variability and long-term survival among elderly people with chronic disease. *Proceedings of the National Academy of Sciences*, 109(17) 6608–6613.

- Zhang, Y., S.S. Isukapalli, L. Bielory, and P.G. Georgopoulos. 2013. Bayesian analysis of climate change effects on observed and projected airborne levels of birch pollen. *Atmospheric Environment*, 68:64-73.
- Ziska, L. K. Knowlton, C. Rogers, D. Dalan, N. Tierney, M.A. Elder, W. Fillery, J. Shropshire, L.B. Ford, C. Hedberg, P. Fleetwood, K.T. Hovanky, T. Kavanaugh, G. Fulford, R.F. Vrtis, J.A. Patz, J. Portnoy, F. Coates, L. Bielory, and D. Frenz. 2011. Recent warming by latitude associated with increased length of ragweed pollen season in central North America. *Proceedings of the National Academy of Sciences*, 108(10): 4248-4251.

Appendix A. Heat Index Calculation

To account for the combined effects of heat and humidity, the National Weather Service (NWS) has adopted the Heat Index, which attempts to calculate the apparent “felt” temperature by adjusting for humidity. NWS calculates the Heat Index only when air temperature is greater than or equal to 80 °F and relative humidity is greater than or equal to 40 percent. Heat Index values are summarized graphically in Figure 10, Section 3. The values shown in that chart are derived from the following mathematical formula:

$$HI = c_1 + c_2T + c_3RH + c_4TRH + c_5T^2 + c_6RH^2 + c_7T^2RH + c_8TRH^2 + c_9T^2RH^2$$

where:

HI = Heat Index (°F),

T = ambient dry bulb temperature (°F), and

RH = relative humidity (%)

and the following constants apply:

$$c_1 = -42.379$$

$$c_2 = 2.04901523$$

$$c_3 = 10.14333127$$

$$c_4 = -0.22475541$$

$$c_5 = -6.83783 \times 10^{-3}$$

$$c_6 = -5.481717 \times 10^{-2}$$

$$c_7 = 1.22874 \times 10^{-3}$$

$$c_8 = 8.5282 \times 10^{-4}$$

$$c_9 = -1.99 \times 10^{-6}$$

Appendix B. Relative Humidity Calculation

The existing climate series developed for *SafeWater* RI included temperature and dew point from the Providence Airport station (COOP ID RI376698) but not relative humidity. Therefore, relative humidity was estimated from temperature and dew point using the August-Roche-Magnus approximation:

$$RH = 100 \frac{\exp\left(\frac{aT_d}{b+T_d}\right)}{\exp\left(\frac{aT}{b+T}\right)}$$

where:

$$a = 17.271,$$

$$b = 237.7,$$

T = air temperature (°C),

T_d = dew point temperature (°C), and

RH = relative humidity (percent).

This approach is considered valid for T between 0 and 60 °C (32 to 140 °F) and T_d between 0 and 50 °C (32 to 122 °F). For cases where the approximation resulted in relative humidity slightly greater than 100 percent, relative humidity was capped at 100 percent.